Article

Structure

Substrate Specificity and Plasticity of FERM-Containing Protein Tyrosine Phosphatases

Graphical Abstract

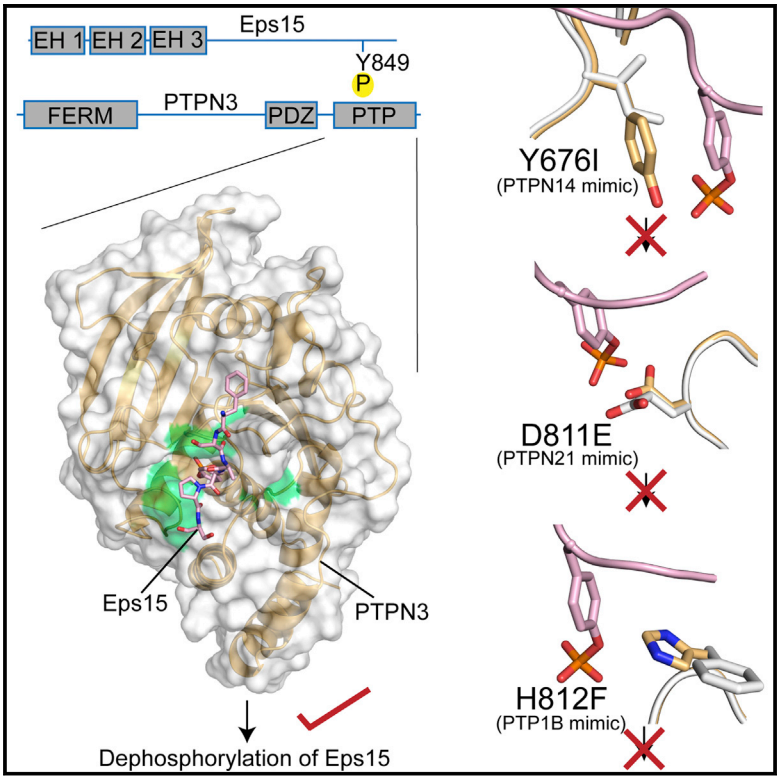

Authors

Kai-En Chen, Meng-Yen Li, ...,
Tzu-Ching Meng, Andrew H.-J. Wang

Correspondence

ahjwang@gate.sinica.edu.tw (A.H.-J.W.),
tcmeng@gate.sinica.edu.tw (T.-C.M.)

In Brief

Eps15 is a newly identified substrate of PTPN3 known to be involved in the regulation of EGFR trafficking. Chen et al. reveal molecular insights into the specific recognition of Eps15 by PTPN3 and members in the FERM domain-containing PTP subfamily comprising PTPN4, N13, N14, and N21.

Highlights

- The recognition of Eps15 as a substrate by PTPN3 is biologically significant
- Pro850 of Eps15 and His812 of PTPN3 plays a central role in substrate specificity
- Identification of residues responsible for substrate specificity in the subfamily
- E811 in WPE loop is unfavorable to act as a general acid during dephosphorylation

Accession Numbers

4RH5
4S0G
4RH9
4RHG
4RI4
4RI5

Chen et al., 2015, Structure *23*, 653–664
April 7, 2015
http://dx.doi.org/10.1016/j.str.2015.01.017

Structure
Article

Substrate Specificity and Plasticity of FERM-Containing Protein Tyrosine Phosphatases

Kai-En Chen,[1] Meng-Yen Li,[1,2] Chia-Cheng Chou,[1,3] Meng-Ru Ho,[1] Guang-Chao Chen,[1,2] Tzu-Ching Meng,[1,2,*] and Andrew H.-J. Wang[1,2,3,4,*]
[1]Institute of Biological Chemistry, Academia Sinica, Taipei 115, Taiwan
[2]Institute of Biochemical Sciences, College of Life Science, National Taiwan University, Taipei 115, Taiwan
[3]National Core Facility for Protein Structural Analysis, Academia Sinica, Taipei 115, Taiwan
[4]Graduate Institute of Translational Medicine, College of Medical Science and Technology, Taipei Medical University, Taipei 110, Taiwan
*Correspondence: ahjwang@gate.sinica.edu.tw (A.H.-J.W.), tcmeng@gate.sinica.edu.tw (T.-C.M.)
http://dx.doi.org/10.1016/j.str.2015.01.017

SUMMARY

Epidermal growth factor receptor (EGFR) pathway substrate 15 (Eps15) is a newly identified substrate for protein tyrosine phosphatase N3 (PTPN3), which belongs to the FERM-containing PTP subfamily comprising five members including PTPN3, N4, N13, N14, and N21. We solved the crystal structures of the PTPN3-Eps15 phosphopeptide complex and found that His812 of PTPN3 and Pro850 of Eps15 are responsible for the specific interaction between them. We defined the critical role of the additional residue Tyr676 of PTPN3, which is replaced by Ile939 in PTPN14, in recognition of tyrosine phosphorylated Eps15. The WPD loop necessary for catalysis is present in all members but not PTPN21. We identified that Glu instead of Asp in the WPE loop contributes to the catalytic incapability of PTPN21 due to an extended distance beyond protonation targeting a phosphotyrosine substrate. Together with in vivo validations, our results provide novel insights into the substrate specificity and plasticity of FERM-containing PTPs.

INTRODUCTION

Signal transduction mediated by reversible tyrosine phosphorylation is an essential process for a diverse array of cellular activities (Tonks, 2006). This fundamental mechanism is controlled by a balance of protein tyrosine kinases, protein tyrosine phosphatases (PTPs), and thousands of their substrates in cells. A prominent feature of PTPs is to regulate both signal activation and termination through the dephosphorylation of receptor tyrosine kinases and their downstream substrates (Julien et al., 2011; Tonks, 2006). Due to such critical functions in vivo, PTPs are associated with various human diseases, including type 2 diabetes, immune disorders, and cancers (Julien et al., 2011; Mustelin et al., 2005; Ostman et al., 2006; Tonks, 2006).

It is known that PTPs execute their regulatory roles in cell signaling through a sophisticated network of interaction with specific substrates (Tiganis and Bennett, 2007; Tonks, 2006). Accumulating evidences have demonstrated that substrate specificity is the key for PTPs to control signal transduction precisely in vivo (Bentires-Alj and Neel, 2007; Elchebly et al., 1999; Julien et al., 2007; Klaman et al., 2000; Salmeen et al., 2000). A high level of the substrate specificity of PTPs can be determined by the conserved catalytic domain (Salmeen et al., 2000; Sarmiento et al., 1998), diverse regulatory domains (Francis et al., 2011; Gray et al., 2003), restricted tissue distribution or subcellular localization (Haj et al., 2002), or various posttranslational modification (PTM) events (Berman-Golan and Elson, 2007; Dadke et al., 2007; Zheng et al., 2000). A classic example of substrate specificity mediated by the PTP catalytic domain is the recognition of the tandem tyrosine motif ($pYpY^{1162-1163}$) of the insulin receptor kinase (IRK) by PTP1B. A structural study showed that the $pTyr^{1162}$ residue binds to the active site of PTP1B, and the adjacent $pTyr^{1163}$ fits within the secondary binding groove (Salmeen et al., 2000). Based on this result, it was proposed that a PTP that does not contain the consensus secondary binding groove may lose its catalytic efficiency and specificity toward IRK (Salmeen et al., 2000). In the case of HePTP, the substrate specificity is primarily determined by the N-terminal kinase interaction motif (KIM) rather than its catalytic domain (Critton et al., 2008; Francis et al., 2011, 2013). Additional studies suggested a critical role of tyrosine phosphorylation at the C-terminal tail of rPTPα and rPTPε in the activation of c-Src through the competitive displacement mechanism (Berman-Golan and Elson, 2007; Zheng et al., 2000). However, the aforementioned examples represent only a small subset of PTPs with identified mechanism of substrate specificity. To date, the molecular basis for substrate recognition by many PTPs remains poorly characterized. Obviously, structures of PTPs in complex with their substrates at a high resolution are essential to delineate the underlying mechanism that determines specific regulation of signaling pathways by PTPs.

Protein tyrosine phosphatase N3 (PTPN3/PTPH1) belongs to a subfamily of five PTPs that contain an N-terminal 4.1 protein, ezrin, radixin, and moesin (FERM) plasma membrane-localization domain and a C-terminal catalytic domain. PTPs in this subfamily can be further divided into two types based on the presence of a PDZ domain. Previous studies reported that PTPN3 is capable of dephosphorylating several substrates (Han et al., 2000; Hou et al., 2010; Zhang et al., 1999), including key regulators heavily involved in the progression of human cancers (Hou et al., 2010; Julien et al., 2011). In addition, we have recently shown that

epidermal growth factor (EGF) receptor (EGFR) pathway substrate 15 (Eps15) is an in vivo substrate of PTPN3 (Li et al., 2014). Eps15 was identified to function as a scaffolding adaptor that regulates endocytosis and trafficking of EGFR (van Bergen En Henegouwen, 2009). It was also known that Eps15 is phosphorylated at Tyr850 (pTyr849 in human) following EGFR activation (Confalonieri et al., 2000). Nonetheless, the biological role of Eps15 was not fully addressed until the demonstration of our study that Tyr850 dephosphorylation of Eps15 by PTPN3 plays a key role in promoting lipid raft-mediated endocytosis and lysosomal degradation of EGFR (Li et al., 2014), and consequently downregulating cell proliferation and tumor growth in lung cancers (Li et al., 2014). These new findings collectively suggest that the specific recognition of Eps15 as a substrate of PTPN3 is biologically relevant.

Because Eps15 does not contain any obvious protein interaction motif that may bind to either the FERM domain or the PDZ domain of PTPN3, we hypothesized that PTPN3-recognized substrate specificity toward Eps15 is determined by the catalytic domain. To elucidate the molecular insight, we have used crystallography and enzyme kinetics to investigate how PTPN3 and Eps15 form an enzyme-substrate complex. Our crystal structure of the PTPN3 catalytic domain together with an Eps15 phosphopeptide reveals an atypical, previously unknown binding orientation. With the complex formation between PTPN3 and Eps15 to be a basis, we further extended our study to highlight key residues responsible for substrate recognition and catalysis of members in this FERM domain-containing PTP subfamily.

RESULTS

Structure of PTPN3$_{PTP}$-Eps15 Phosphopeptide Complexes

A synthetic peptide that corresponds to the tyrosine phosphorylation segment of human Eps15 (Eps15$^{846–854}$) was generated for cocrystallization with the entire phosphatase domain (N3$_{PTP}$) of human PTPN3 (Figure 1A). To facilitate the formation of a stable complex with tyrosine phosphorylated substrates, two essential residues of PTPN3 for catalysis, D811 and C842, were mutated to alanine and serine, respectively, according to our previous study (Chen et al., 2014). Crystal structure of N3$_{PTP}$ D811A/C842S mutants in complex with Eps15$^{846–854}$ (hereafter designated as the N3$_{PTP}$ D811A/C842S-Eps15$^{846–854}$ complex structure) was phased by molecular replacement and refined to 1.6 Å resolution (Figure 1B; Table 1). The crystal structure revealed a 1:1 complex in which Eps15$^{846–854}$ was inserted into the PTP active site pocket forming the interaction with the pY, WPD, PTP and Q-loops of PTPN3 (Figures 1B and 1C). Six residues (F846–S851) of Eps15$^{846–854}$ are clearly delineated in the electron density map of the N3$_{PTP}$ D811A/C842S-Eps15$^{846–854}$ complex structure (Figure 1C). However, the electron density for residues 852–854 at the C terminus of Eps15$^{846–854}$ is invisible, suggesting a segment with structural flexibility. To determine whether additional amino acids are involved in the interaction with N3$_{PTP}$, we synthesized a lengthy Eps15 phosphopeptide with 23 residues (Eps15$^{836–858}$) and compared its binding affinity with PTPN3 with the original short form of Eps15$^{846–854}$. Based on the fluorescence polarization assay, the values of the dissociation constant, K_d, for N3$_{PTP}$ D811A/C842S with the lengthy and short Eps15 phosphopeptides are rather similar (Figure S1), suggesting that the residues between 846 and 854 are sufficient to accommodate the active site of N3$_{PTP}$.

The Atypical Binding Conformation of Eps15 Is Mediated by Its pTyr-Pro Motif

As revealed by the superposition of the N3$_{PTP}$ D811A/C842S-Eps15$^{846–854}$ complex structure with other known PTP-phosphopeptide structures (Table S1), the C terminus of Eps15$^{846–854}$ shows an atypical orientation (Figure 1D). We noticed that the first residue on the C terminus of the pTyr849 is a proline (hereafter designated as P^{+1}), which forms a pTyr-Pro motif with the pY^{+0} as a *trans* isomer (Figures 1C and 1D). Due to the unique characteristic of proline, in which the side chain is cyclized into its nitrogen backbone, the psi and phi angles of the peptide bond have fewer allowable degrees of rotation, thus rendering limited conformation of P^{+1} (Figures 1C and 1D). To gain insights into the role of proline in determining substrate specificity, we resolved the structure of N3$_{PTP}$ D811A/C842S in complex with a mutant form of Eps15 phosphopeptide in which proline at the P^{+1} position was replaced by a valine (hereafter designated as the N3$_{PTP}$ D811A/C842S-Eps15$^{846–854}$ P850V complex structure, Table 1). We selected valine rather than other residues because of the presence of valine at the P^{+1} position of p38γ, a known substrate of PTPN3 (Chen et al., 2014). The substitution of proline to valine induced a 3.8 Å shift of the pTyr-Pro motif (Figures 1E and S2). As a result, an additional hydrogen bond was formed with the carboxyl side chain of D678 on the pY loop (Figure 1F), leading to a 1-fold decrease in K_m compared with the wild-type Eps15$^{846–854}$ (Figure 1G). Clearly, the proline at the P^{+1} position is necessary to maintain the atypical orientation of the pTyr-Pro motif. In the absence of proline, Eps15 forms a complex with PTPN3 in an orientation consistent with other known structures (Critton et al., 2008; Phan et al., 2003; Salmeen et al., 2000; Yu et al., 2011).

H812 of PTPN3 Is Required for the Recognition of Eps15

In addition to the pTyr-Pro motif, we observed an unusual stacked-like interaction between the pyrrolidine ring of P^{+1} and the imidazole ring of H812 (Figures 1C and 1F). The carbonyl group of P^{+1} also formed hydrogen bonds with the side chain of H812 and Q886 (Figure S3A), suggesting that these two residues might be necessary for accommodating the atypical orientation of the pTyr-Pro motif of Eps15. We notice that the catalytically essential Q886 is conserved between PTPN3 and PTP1B (Q262 in PTP1B, Figure 2A); however, the position of H812 in PTPN3 is a phenylalanine (F182) in PTP1B (Figure 2A). To test whether the presence of H812 is important to determine substrate specificity, we measured the phosphatase activity between two PTPs against Eps15 phosphopeptides. Our results demonstrated that the catalytic domain of PTP1B could not dephosphorylate Eps15$^{846–854}$ or Eps15$^{836–858}$ efficiently compared with wild-type N3$_{PTP}$ (Figure 2B), supporting a critical role of H812 in recognition of Eps15.

To examine whether H812 is necessary for determining substrate specificity, we solved the structure of a D811A/H812F/C842S/M883G mutant form of N3$_{PTP}$, which acts as a surrogate of the PTP1B$_{PTP}$ active site, in complex with Eps15$^{846–854}$ (Table 1), hereafter designated as the quadruple mutant-Eps15$^{846–854}$

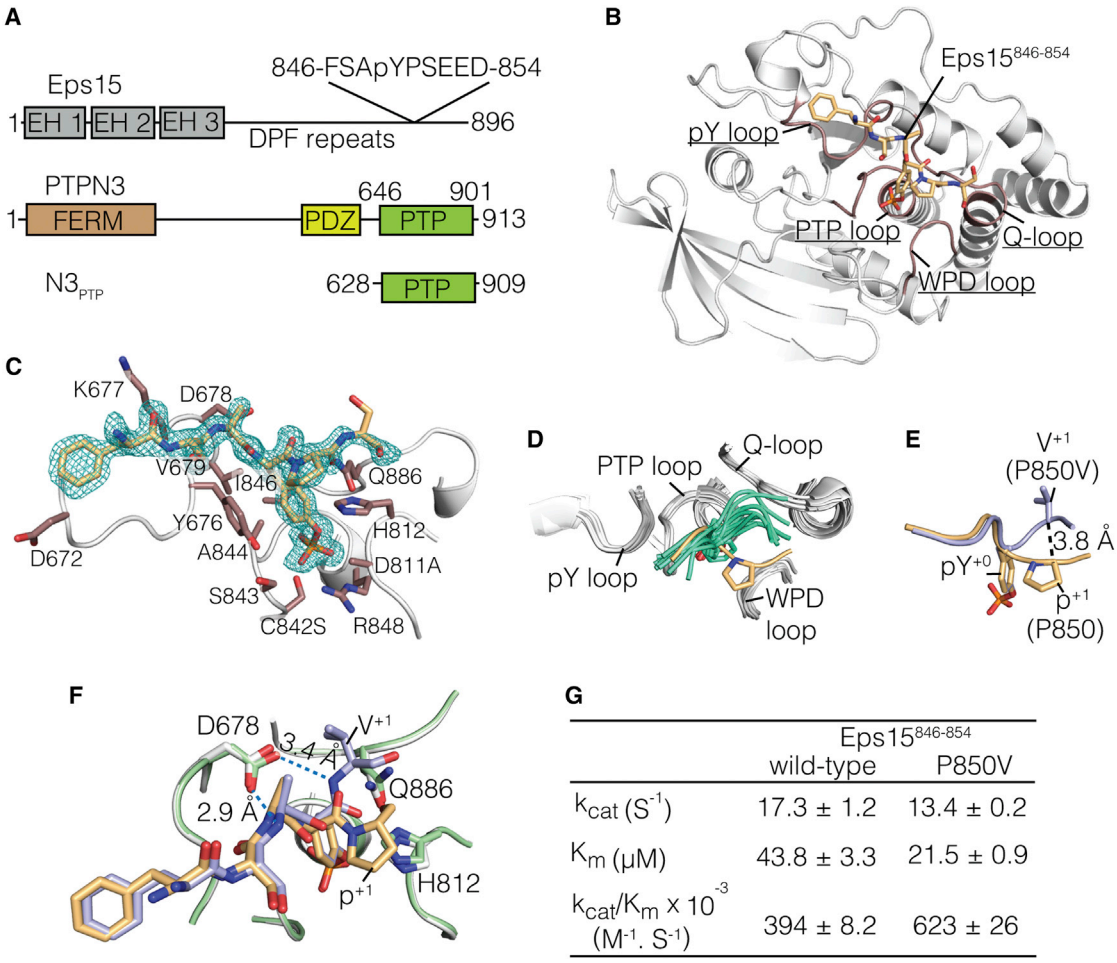

G

	Eps15$^{846-854}$	
	wild-type	P850V
k_{cat} (S^{-1})	17.3 ± 1.2	13.4 ± 0.2
K_m (μM)	43.8 ± 3.3	21.5 ± 0.9
$k_{cat}/K_m \times 10^{-3}$ ($M^{-1}. S^{-1}$)	394 ± 8.2	623 ± 26

Figure 1. Crystal Structure of the N3$_{PTP}$ D811A/C842S-Eps15$^{846–854}$ Complex

(A) Schematic showing the synthetic Eps15 and PTPN3 constructs used in this study.

(B) Cartoon representation of the N3$_{PTP}$ D811A/C842S-Eps15$^{846–854}$ complex. Eps15$^{846–854}$ is highlighted as a light orange stick.

(C) Location of the bound Eps15$^{846–854}$ on the active site of N3$_{PTP}$. Residues of PTPN3 contributing to the interaction are shown as a stick. The electron density shown corresponds to a simulated-annealing OMIT $F_o - F_c$ map contoured at 3σ.

(D) Superposition of the PTP-phosphopeptide complexes. PTPs are highlighted in white, Eps15$^{846–854}$ is highlighted in light orange and other phosphopeptides are highlighted in green cyan.

(E) Superposition of P850 (light orange stick) and P850V (light purple stick) Eps15$^{846–854}$ from the two N3$_{PTP}$ D811A/C842S complexes.

(F) Highlight interactions between D678 and P850 or P850V containing Eps15$^{846–854}$. Substitution of P850 at the P^{+1} position to a valine induced two hydrogen bonds (blue dash line) with D678.

(G) Kinetic parameters of N3$_{PTP}$ using wild-type and P850V mutant of Eps15$^{846–854}$ as a substrate. Error bars represent the SEM for at least three independent assays.

See also Figures S1 and S2, and Table S1.

complex. We noticed that the introduction of M883G substitution increased the flexibility of the side chain of Q886, thus facilitating interaction between F812 and the pTyr-Pro motif (Figures 2C and 2D). In this complex structure, the phenyl side chain of F812 is shifted 3.7 Å away from the active site pocket (Figures 2C and 2D). Instead of forming a stacked-like contact to P^{+1}, the phenyl side chain of F812 established a hydrophobic interaction with the main chain of E^{+3} (E852) and E^{+4} (E853) in Eps15 (Figure S3B). When modeling the phenyl side chain of F812 to the position at which the imidazole ring of H812 is located, we found a steric repulsion with the carbonyl group of P^{+1} (Figure S3B). To avoid this repulsion, F812 shifts away and the contacts to P^{+1} of Eps15 are lost, resulting in the formation of a much looser active site pocket compared with the wild-type N3$_{PTP}$ (Figures 2E and 2F). As a consequence, there were a 6-fold increase in K_m and a 2-fold decrease in k_{cat} when we substituted phenylalanine for H812 in the kinetic assay of PTPN3 against Eps15 (Table 2). Interestingly, this H812F mutant form of N3$_{PTP}$ behaved similarly to the wild-type PTP1B$_{PTP}$, which showed a 9-fold increase in K_m and a 3.6-fold decrease in k_{cat} relative to the wild-type N3$_{PTP}$ (Table 2) In the reciprocal experiment, we measured Eps15$^{846–854}$ dephosphorylation catalyzed by the F182H mutant form of PTP1B$_{PTP}$. Clearly, the substitution of histidine for F182 led to a 1-fold increase of k_{cat} over its wild-type (Table 2), suggesting

Table 1. Data Collection and Refinement Statistics

Data Collection	$N3_{PTP}$ D811A/C842S + $Eps15^{846–854}$	$N3_{PTP}$ D811A/C842S + $Eps15^{846–854}$ P850V	Quadruple Mutant + $Eps15^{846–854}$	$N3_{PTP}$ D811E/C842S + $Eps15^{846–854}$	$N3_{PTP}$ Y676I	$N3_{PTP}$ D811E
PDB ID	4RH5	4S0G	4RH9	4RHG	4RI4	4RI5
Space group	$P2_12_12_1$	$P2_12_12_1$	$P2_12_12_1$	$P2_12_12_1$	$C222_1$	$C222_1$
Resolution (Å)	30.00–1.60 (1.66–1.60)[a]	50.00–1.72 (1.78–1.72)[a]	50.00–1.60 (1.66–1.60)[a]	30.00–1.58 (1.64–1.58)[a]	30.00–1.60 (1.66–1.60)[a]	30.00–1.26 (1.31–1.26)[a]
a, *b*, *c* (Å)	57.9, 67.5, 69.6	58.1, 67.3, 68.9	58.1, 67.6, 69.8	58.2, 67.7, 70.0	94.9, 99.4, 134.3	95.2, 96.1, 141.7
α, β, γ (°)	90.0, 90.0, 90.0	90.0, 90.0, 90.0	90.0, 90.0, 90.0	90.0, 90.0, 90.0	90.0, 90.0, 90.0	90.0, 90.0, 90.0
Total observations	278,642	110,529	223,125	258,564	588,490	865,617
Unique, reflections	36,684	28,900	34,544	37,336	83,163	170,606
Completeness	99.8% (99.6%)[a]	99.0 (99.4)[a]	93.1% (97.3%)[a]	97.0% (100.0%)[a]	99.1% (97.7%)[a]	97.9% (90.3%)[a]
R_{merge}[b]	0.06 (0.36)[a]	0.068 (0.52)[a]	0.10 (0.60)[a]	0.04 (0.21)[a]	0.06 (0.54)[a]	0.04 (0.42)[a]
$\langle I/\sigma(I)\rangle$	31.8 (4.8)[a]	15.0 (2.1)[a]	13.5 (3.4)[a]	39.8 (8.9)[a]	25.8 (3.5)[a]	37.1 (2.2)[a]
Multiplicity	7.6 (7.4)[a]	3.8 (3.9)[a]	6.5 (6.6)[a]	6.9 (7.3)[a]	7.1 (6.4)[a]	5.1 (4.5)[a]
Refinement Statistics						
R_{work}/R_{free} (%)[c,d]	17.4/20.4	18.2/22.9	19.5/22.6	18.3/20.9	16.3/18.9	15.9/17.3
No. of Non-H Atoms						
Protein + ligand	2593	2303	2567	2593	5149	5611
Waters	261	139	206	212	543	873
Wilson B ($Å^2$)	14.7	19.5	18.0	17.9	20.6	15.4
Average B ($Å^2$)	20.2	28.8	26.0	25.2	27.4	23.3
RMSD bonds (Å)	0.012	0.012	0.011	0.010	0.010	0.011
RMSD angles (°)	1.42	1.31	1.41	1.19	1.29	1.39
Ramachandran Plot						
Favored (%)[e]	96.9	96.5	94.9	96.6	97.1	96.5
Outliers (%)[e]	0.3	0.4	0.3	0.3	0.3	0.5

[a]Values in parentheses refer to the highest resolution shell.
[b]$R_{merge} = \sum|I-\langle I\rangle|/\sum\langle I\rangle$, where I is the intensity of each individual reflection.
[c]$R_{work} = \sum_h|F_o - F_c|/\sum_I|F_o|$, where F_o and F_c are the observed and calculated structure-factor amplitudes for each reflection h.
[d]R_{free} was calculated with 10% of the diffraction data selected randomly and excluded from refinement.
[e]Calculated using Molprobabity.

that a histidine instead of a phenylalanine at the 182 position improves the substrate selectivity of PTP1B toward Eps15 (Figures S3C and S3D). On the other hand, the minor decrease of K_m indicates that additional residues near the active site of PTP1B might have impaired its ability to recognize Eps15.

Analysis of PTPN13 and PTPN14 within the FERM Domain-Containing PTP Subfamily

Due to the presence of plasma membrane-localized FERM domain, all members within this PTP subfamily may have the access to tyrosine phosphorylated Eps15, which is in complex with the receptor tyrosine kinase EGFR in cells. Using the knowledge of structural insights that depict the substrate specificity determined by PTPN3, we investigated in the next phase of study whether an additional four FERM domain-containing PTPs can function as Eps15 phosphatases. Analysis of sequence alignment indicated that H812 is absolutely conserved throughout the subfamily (Figures 3 and S4), highlighting a critical role of this residue in substrate recognition among all five members. In the case of PTPN4, we noticed that all necessary residues around the active site for catalysis are conserved with PTPN3 (Figure 3). In addition, the overall sequence identity inside the catalytic domains of PTPN3 and PTPN4 reaches 62%. These features suggest that substrate specificity between the two phosphatases may be determined by regions outside the catalytic domain, and thus, the detailed investigation is beyond the scope of our present study. PTPN13 has been reported to be a PTP1B-like enzyme (Villa et al., 2005) due to the presence of G2449 (Figure 3) in the secondary binding pocket (G259 in PTP1B, shown in Figure 2A). However, PTPN13 binds to $Eps15^{846–854}$ more strongly than PTP1B (Table 3, compared with Table 2), largely because of the unique H2379 responsible for substrate recognition (Figure 3). The other difference that we noticed is an aspartic acid (D2380) in PTPN13 instead of a glycine residue in PTPN3 inside the WPD loop (Figure 3). The presence of an additional aspartic acid suggests that the side chain of H2379 in PTPN13 might interact with the side chains of D2378 and D2380. Such interaction likely causes a perturbation of H2379, rendering this particular residue unable to form a stable stacked-like contact to $Eps15^{846–854}$. As a result, we observed a 3-fold increase in K_m of the wild-type $PTPN13_{PTP}$ compared with $N3_{PTP}$ (Table 3).

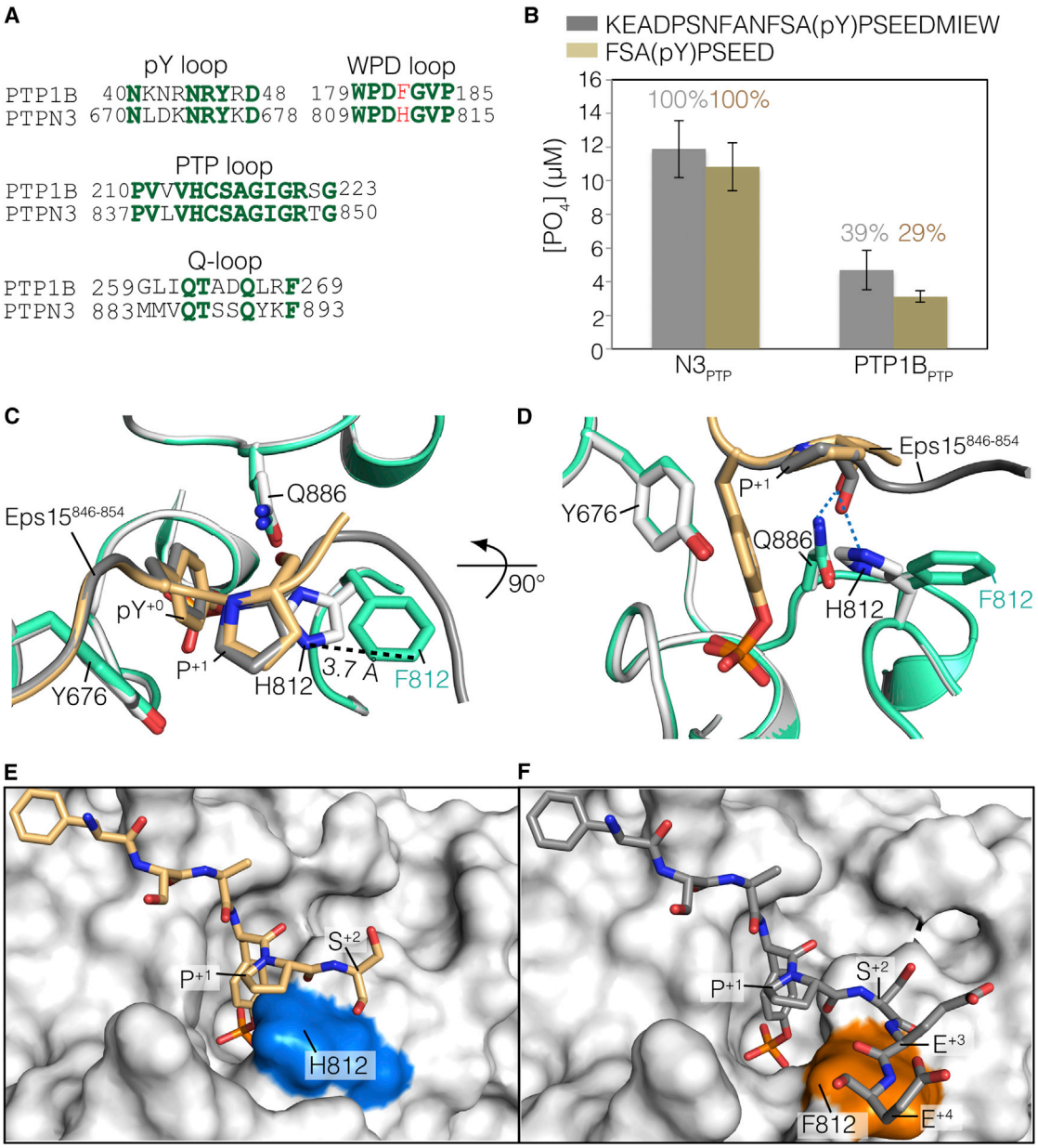

Figure 2. Comparison of H812 and F812 in the Recognition of Eps15$^{846–854}$

(A) Sequence alignment of PTPN3 and PTP1B showing the pY loop, WPD loop, PTP loop, and Q-loop. Conserved residues are highlighted in green, and key variable residues, F182 and H812, are highlighted in red. Sequence alignment was generated using CLUSTALW from Network Protein Sequence Analysis using default parameters (Combet et al., 2000).

(B) Phosphatase activity of the wild-type N3$_{PTP}$ and PTP1B$_{PTP}$ toward two different Eps15 phosphopeptide substrates. The assay was performed using 10 nM of protein with 50 μM of Eps15 phosphopeptides. Error bars represent the SEM for at least three independent assays.

(C) Highlight of the active site of the N3$_{PTP}$ D811A/C842S-Eps15$^{846–854}$ complex structure (white) superposed with the quadruple mutant-Eps15$^{846–854}$ complex structure (green cyan).

(D) Superposition rotated 90° around the horizontal axis of (C) to show the hydrogen bonds of the carbonyl group of P^{+1} to the side chains of H812 and Q886 (indicated as brown dashed lines).

(E) Molecular surface of the N3$_{PTP}$ D811A/C842S-Eps15$^{846–854}$ complex structure highlights H812 (blue).

(F) The quadruple mutant-Eps15$^{846–854}$ complex structure highlights F812 (orange).

See also Figure S3.

In the case of PTPN14, the noticeable difference is a substitution of tyrosine in the pY loop with an isoleucine (Figure 3). Previous study has found that the substitution of Y46 with alanine in PTP1B resulted in a 380-fold increase in K_m using *p*NPP as a substrate (Sarmiento et al., 1998). Consistently, in the absence of this critical tyrosine, the wild-type PTPN14$_{PTP}$ is catalytically

Table 2. Kinetic Parameters of $PTP1B_{PTP}$, $N3_{PTP}$, and the Reciprocal Mutants Using $Eps15^{846–854}$ as a Substrate

Enzyme	k_{cat} (s^{-1})	K_m (μM)	$k_{cat}/K_m \times 10^{-3}$ (M^{-1} s^{-1})
$N3_{PTP}$ with $Eps15^{846–854}$			
Wild-type	17.3 ± 1.2	43.8 ± 3.3	394 ± 8.2
H812F	8.9 ± 0.4	260.3 ± 15.3	34 ± 2
$PTP1B_{PTP}$ with $Eps15^{846–854}$			
Wild-type	4.8 ± 1.1	387.9 ± 11.7	12 ± 2.6
F182H	8.1 ± 1.9	317.2 ± 10.9	34 ± 2.0

inactive when four structurally characterized phosphopeptides were used as the substrate in the assay (Figure 4A; Table 3). Interestingly, the Y676I mutant form of $N3_{PTP}$ also lost the catalytic activity completely (Figure 4A). To further improve our understanding of the necessary role of this tyrosine residue in catalysis, we solved the structure of the $N3_{PTP}$ Y676I mutant in complex with sodium orthovandate (Table 1), hereafter designated as the $N3_{PTP}$ Y676I mutant structure. The electron density of I676 and sodium orthovandate is well defined (Figure S5). Using the phosphopeptide $Eps15^{846–854}$ to model the interaction with the active site pocket of the $N3_{PTP}$ Y676I mutant structure, we found that the Cγ2 atom of I676 is too close toward the backbone amide nitrogen of pY^{+0} (Figures 4B and 4C), likely causing a steric repulsion. We propose that such repulsive force is unfavorable for the phosphotyrosine substrate to fit into the deep narrow active site of PTP, leading to a loss of enzymatic activity.

Unique Structural Feature of PTPN21 Reveals a Key Role of the Glutamic Acid in the WPE Loop

It has been well understood that a conserved aspartic acid, which functions as a general acid for nucleophilic attack on the substrate in the first step of catalysis, must appear in the WPD loop among active PTPs. However, this critical residue in PTPN21 is substituted with a glutamic acid, thus resulting in a WPE loop instead (Figure 3). Because of the similarity of chemical characters between aspartic acid and glutamic acid, the WPE loop in PTPN21 might preserve key features for catalysis. On the other hand, a lengthier side chain of glutamic acid compared with aspartic acid could make a unique microenvironment constructed by the WPE loop. With such uncertainties, it is difficult to predict whether PTPN21 is able to recognize $Eps15^{846–854}$ as a substrate. To address this question, we characterized the WPE loop using PTPN3 as a model. The aspartic acid 811 was replaced by a glutamic acid on the backbone of C842S mutant form of $N3_{PTP}$. The phosphopeptide $Eps15^{846–854}$ was complexed with this $N3_{PTP}$ D811E/C842S mutant protein, and then subjected to X-ray crystallography. Examining the details of our structure (Table 1), hereafter designated as the $N3_{PTP}$ D811E/C842S-$Eps15^{846–854}$ complex structure, we observed clear density of the phosphopeptide and WPE loop in a close conformation (Figure S6), which to our knowledge has never been reported previously.

We noticed that the side chain of E811 in the $N3_{PTP}$ D811E/C842S-$Eps15^{846–854}$ complex structure is shifted toward K753 in the E-loop (Figures 5A and 5B). Remarkably, the presence of E811 extended protonation distance targeting the P-O bond of pY^{+0} to 4.7 Å compared with 2.5 Å in the $N3_{PTP}$ D811A/C842S-$Eps15^{846–854}$ complex structure in which D811 was modeled (Figures 5A and 5B). If the side chain of E811 moved closer toward the P-O bond, a steric clash would occur due to an extra methylene group in the glutamic acid. Interestingly, the imidazole ring of H812 in the $N3_{PTP}$ D811E/C842S-$Eps15^{846–854}$ complex structure exhibits an alternative conformation that shifts 2.3 Å outward from the active site, likely due to the perturbation caused by E811 (Figure 5A), which led to a 3-fold increase in the K_m of the D811E mutant (Table 3). Moreover, our kinetic study indicated that substitution of D811 with glutamic acid in PTPN3 resulted in an 870-fold reduction of k_{cat} (Table 3). Consistently, we were unable to detect any activity for the WPE loop-containing constructs, no matter whether *p*NPP (Figure 5C) or $Eps15^{846–854}$ (Figure 5D) was used as a substrate in the phosphatase activity assay. Interestingly, once the glutamic acid in the WPE loop was replaced by an aspartic acid, the E1067D mutant form of $PTPN21_{PTP}$ exhibited a significantly higher level of phosphatase activity compared with its wild-type counterpart (Figures 5C and 5D). The data demonstrate that the WPE loop is a key region responsible for the catalytic inertness of PTPN21.

Our results demonstrated that the glutamic acid of the WPE loop is located in an unfavorable position, so it cannot act as a general acid in the first step of the dephosphorylation process. We then investigated whether this glutamic acid forms a hydrogen bond with the nucleophilic water molecule, similar to how the aspartic acid of the WPD loop functions in the hydrolysis step during substrate dephosphorylation. For this, we crystallized the D811E mutant form of $N3_{PTP}$ in the presence of a 1-fold molar excess of sodium orthovanadate. The structure of the $N3_{PTP}$ D811E single mutant (Table 1), hereafter designated as the $N3_{PTP}$ D811E mutant structure, solved at 1.25 Å reveals an unusual trigonal planar shape of electron density around the thiol group of C842 (Figure 5E). Different from the trigonal bipyramidal shape density of orthovanadate in the $N3_{PTP}$ Y676I mutant structure, the density shown in the $N3_{PTP}$ D811E mutant structure is likely to be a metavanadate (Figure 5E). Typically, the orthovanadate is formed due to attack of the nucleophilic water positioned by catalytically essential glutamine and aspartic acid of the Q-loop and WPD loop, respectively (Pannifer et al., 1998) (Figure 5F). However, we observed that E811 in the $N3_{PTP}$ D811E mutant is out of the position to facilitate Q886 in coordination of the nucleophilic water molecule, thus explaining why a metavanadate molecule was formed (Figure 5G). Collectively, our structural findings provide an underlying mechanism of how the WPE loop of PTPN21 is incapable of coordinating with the nucleophilic water molecule during the dephosphorylation process.

H812 and D811 in PTPN3 Are Essential for Regulating Eps15-Dependent EGFR/MAPK Signaling In Vivo

The critical roles of H812 and D811 in substrate recognition and efficient catalysis of PTPN3-mediated Eps15 dephosphorylation have been clearly delineated by structural approaches (Figures 2 and 5) and enzyme kinetic analyses (Tables 2 and 3). We next tested whether the presence of these two residues is essential for PTPN3 to regulate Eps15-dependent EGFR signaling in cultured cells. Transfection of human embryonic kidney HEK293T cells with the wild-type PTPN3 significantly decreased EGF-induced Y849 phosphorylation of Eps15, whereas ectopic expression of the D811E or H812F mutant

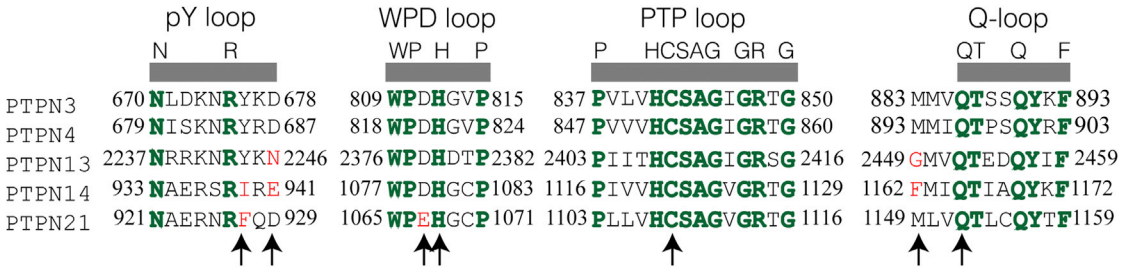

Figure 3. Sequence Alignment of FERM Domain-Containing PTPs against PTP1B Showing the pY Loop, WPD Loop, PTP Loop, and Q-Loop
Conserved residues are highlighted in green and labeled on top. Key variable residues are highlighted in red. Key residues discussed in this study are indicated with an arrow. Sequence alignment was generated using Clustal W from Network Protein Sequence Analysis using default parameters (Combet et al., 2000). See also Figure S4.

form of PTPN3 did not affect the Y849 phosphorylation levels of Eps15 (Figure 6A). Furthermore, in the H1975 line derived from human non-small-cell lung cancer, in which the wild-type form of PTPN3 could downregulate EGFR signaling via dephosphorylating Eps15 (Li et al., 2014), we found that ectopic expression of the D811E or H812F mutant form of PTPN3 failed to reduce the level of endogenous EGFR and the phosphorylation of mitogen-activated protein kinase (MAPK) in response to EGF stimulation (Figures 6B and 6C). These results suggest that, when expressed in H1975 cells, both mutant forms of PTPN3 were incapable of dephosphorylating Eps15 efficiently, consequently leading to the accumulation of EGFR and constitutive activation of the downstream MAPK signaling pathway.

DISCUSSION

We investigated the molecular basis that determines the specific interaction between PTPN3 and Eps15, both of which function coordinately to regulate endocytosis and degradation of EGFR. The structural analysis revealed critical roles of the H812 in the phosphatase domain of PTPN3 and the pTyr-Pro motif of Eps15 responsible for the formation of the PTPN3-Eps15 complex. We showed that the stacked-like interaction drives the binding of H812 specifically to the P^{+1} position of the pTyr-Pro motif. The substitution of H812 with phenylalanine in PTPN3 resulted in a loss of Eps15 recognition without significantly altering its catalytic activity, confirming the substrate specificity determined by this particular residue. Although the conserved His residue is present in all five PTPs belonging to the same subfamily with a FERM domain, diversities in the pY loop, WPD loop, and Q-loop occur among these members. We demonstrated an essential role of the tyrosine residue in the pY loop of PTPN3 for a robust interaction with specific substrates. PTPN14 that has an isoleucine instead of a tyrosine in the pY loop loses the binding affinity to Eps15. A combination of structural study and enzymatic kinetic analysis further indicates that an aspartic acid (D811 in PTPN3) in the WPD loop is absolutely required for PTP-mediated substrate dephosphorylation. The presence of a glutamic acid instead of an aspartic acid in the WPE loop renders PTPN21 to retain its ability for substrate recognition. However, this glutamic acid located in the active site of the phosphatase domain is structurally unfavorable to function as a general acid, thus significantly reducing the catalytic activity of PTPN21. Further in vivo evidence depicted that both the H812F and D811E mutant forms of PTPN3 cannot regulate the Eps15-dependent EGFR/MAPK signaling pathway in response to EGF stimulation, validating the structural insights demonstrated in our study. In addition to Eps15, we have identified seven phosphotyrosine proteins that share a common pTyr-Pro motif (Table S2). New findings shown in the current work open an avenue toward delineating specific recognition of other putative substrates by PTPN3.

Our data suggest that the conserved histidine residue located in the WPD loop of FERM domain-containing PTPs plays a key role in recruiting Eps15 as a substrate. However, the presence of this histidine alone may not be sufficient enough to determine the substrate specificity of PTPs. Recent studies have used the approach of peptide library screening to search for sequence specificity that pairs a PTP and its substrate (Barr et al., 2009; Ren et al., 2011). One report using such an approach aimed to characterize the substrate specificity of Lyp, a PTP containing a histidine in the WPD loop (Yu et al., 2011). Interestingly, the study identified an overall preference for acidic residues instead of a proline at the P^{+1} position of the potential substrates of Lyp (Yu et al., 2011). This finding suggests that, even although a given PTP contains a histidine residue in the WPD loop, it may not recognize Eps15 as a substrate. We propose that a complete interaction network formed by not only the histidine but also other key residues in the phosphatase domain is required to perfectly coordinate with the pTyr-Pro motif of Eps15.

Three residues, including M883 in the Q-loop, Y676 in the pY loop, and D811 in the WPD loop, which are present in PTPN3 but are replaced by various amino acids among other PTPs in the same subfamily, were investigated for their roles in determining substrate specificity. We showed that the binding affinity of $PTPN13_{PTP}$ for $Eps15^{846–854}$ is weaker than $N3_{PTP}$. A possible reason for that is the presence of G2449 in the Q-loop of PTPN13, instead of M833 at the same position in PTPN3. Interestingly, a previous study suggested that G2449 in the Q-loop facilitates the formation of a secondary binding pocket, thus promoting the preference of dual phosphorylated substrates for PTPN13 (Villa et al., 2005). Nonetheless, the impact of this particular substitution to the determination of substrate specificity among PTPs requires further investigation.

To date, the structural basis for substrate recognition of PTPN14 has been poorly understood (Wadham et al., 2003; Zhang et al., 2013). PTPN14 is the only nonreceptor PTP that contains an isoleucine instead of an aromatic residue in the pY loop

Table 3. Kinetic Parameters of D811E, Y676I and FERM Domain-Containing PTPs Using Eps15$^{846–854}$ as a Substrate

Enzyme	k_{cat} (s^{-1})	K_m (μM)	$k_{cat}/K_m \times 10^{-3}$ (M^{-1} s^{-1})
$N3_{PTP}$			
Wild-type	17.3 ± 1.2	43.8 ± 3.3	394 ± 8.2
Y676I	ND	ND	–
D811E	0.019 ± 0.002	131.4 ± 1.6	0.10 ± 0.01
$PTPN13_{PTP}$			
Wild-type	14.0 ± 0.5	140.3 ± 8.0	100 ± 2
$PTPN14_{PTP}$			
Wild-type	ND	ND	–

ND, no phosphatase activity detected.

(Sarmiento et al., 1998). Examining the structural insights of the $N3_{PTP}$ Y676I mutant, we observed a close proximity between the methyl side chain of I676 and the main chain of pY^{+0} in the substrate, indicating a high degree of difference in the substrate recognition process between PTPN3 and PTPN14. Importantly, a number of phosphoproteins without sequence similarity to Eps15, such as β-catenin (Wadham et al., 2003), YAP (Liu et al., 2013), and p130Cas (Zhang et al., 2013), were found to be potential substrates of PTPN14. Additional studies are needed to reveal whether the unique structure of I939 in the pY loop plays a key role in coordinating with specific substrates of PTPN14.

Among nonreceptor PTPs, PTPN21 and PTPN23 are the only two members that have a WPE loop instead of a WPD loop. Using structural approaches, we demonstrated how the substitution of aspartic acid with glutamic acid causes a loss of proton donation to substrate, thus providing the underlying mechanism of catalytic inertness of PTP21 and PTPN23 reported previously (Barr et al., 2009; Gingras et al., 2009). On the other hand, many receptor PTPs (rPTPs) have a WPE loop in their membrane-proximal domain (D2 domain). In fact, it has been reported that D2 domains of these rPTPs exhibit low or no catalytic activity (Andersen et al., 2001; Streuli et al., 1990; Wang and Pallen, 1991), even although their overall three-dimensional fold shows similar features to the catalytically active D1 domain (Streuli et al., 1990). Clearly, our results provide the first structural basis that rationally explains why those WPE loop-containing D2 domains in rPTPs are catalytically inert.

In conclusion, our findings not only identify key residues in the phosphatase domain that determine specific interaction between PTPN3 and Eps15 but also provide structural interpretations on how the substrate plasticity is achieved among FERM-containing PTPs. The molecular insights presented in this study will enable rational drug design to treat human diseases that are associated with dysfunction of these five PTPs.

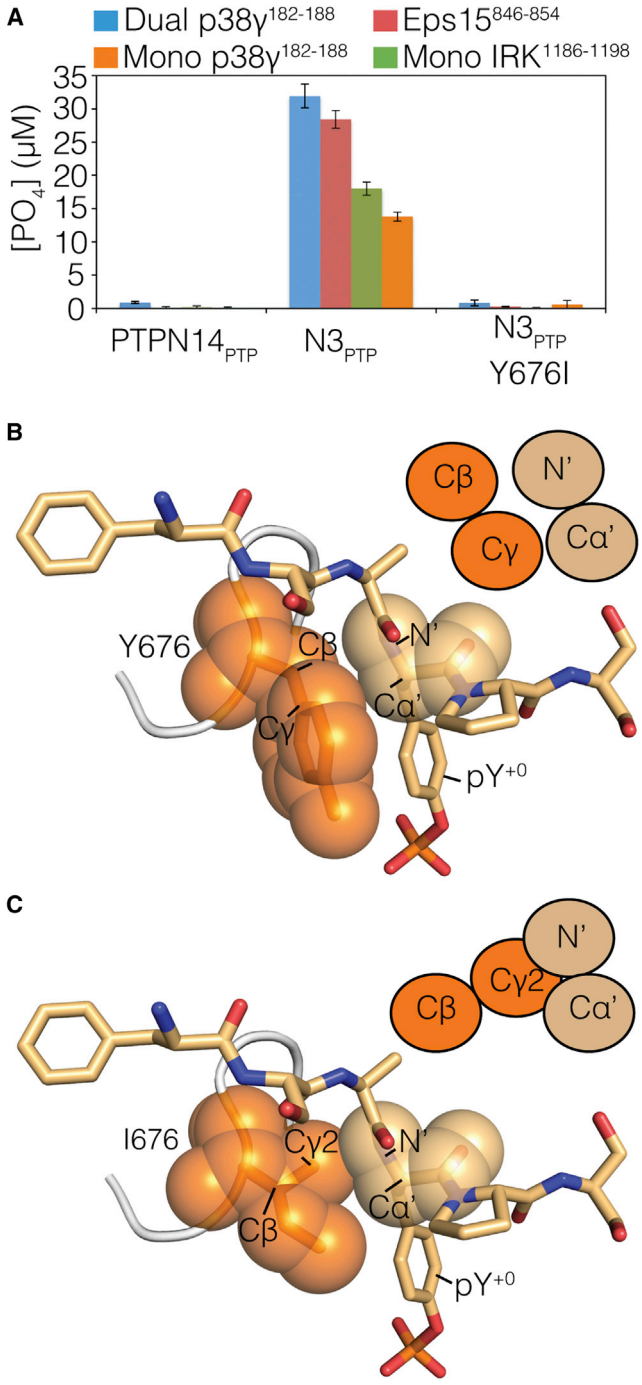

Figure 4. Y676I Substitution Causes Steric Repulsion with Eps15$^{846–854}$

(A) Phosphatase activity of the wild-type $PTPN14_{PTP}$, $N3_{PTP}$, and the Y676I mutant of $N3_{PTP}$ using four different phosphopeptides as substrate. The assay was performed using 20 nM protein with 200 μM phosphopeptides. Error bars represent the SEM for at least three independent assays.

(B and C) (B) Highlight of Y676 from the $N3_{PTP}$ D811A/C842S-Eps15$^{846–854}$ complex and (C) I676 from the $N3_{PTP}$ Y676I mutant structure. For clarity, Eps15$^{846–854}$ in (C) was modeled from the $N3_{PTP}$ D811A/C842S-Eps15$^{846–854}$ complex. The sphere represents the van der Waals radius of each atom of Y676, I676, and the main chain of pY^{+0}. The schematic illustrates the side chain atoms in close contact, shown in the top left corner.

See also Figure S5.

EXPERIMENTAL PROCEDURES

Plasmid Construction and Site-Directed Mutagenesis

PCR fragments of $N3_{PTP}$ (residues 628–909), $PTP1B_{PTP}$ (residues 1–320), $PTPN4_{PTP}$ (residues 611–926), $PTPN13_{PTP}$ (residues 2163–2467), $PTPN14_{PTP}$ (residues 886–1187), and $PTPN21_{PTP}$ (residues 872–1174) were amplified from the full-length human PTPN3-, PTP1B-, PTPN4-, PTPN13-, PTPN14-, and PTPN21-encoded genes, respectively. All amplified gene products were ligated into an N-terminal His-tag pMCSG7 vector using ligation independent cloning (Stols et al., 2002). Site-directed mutagenesis was used to

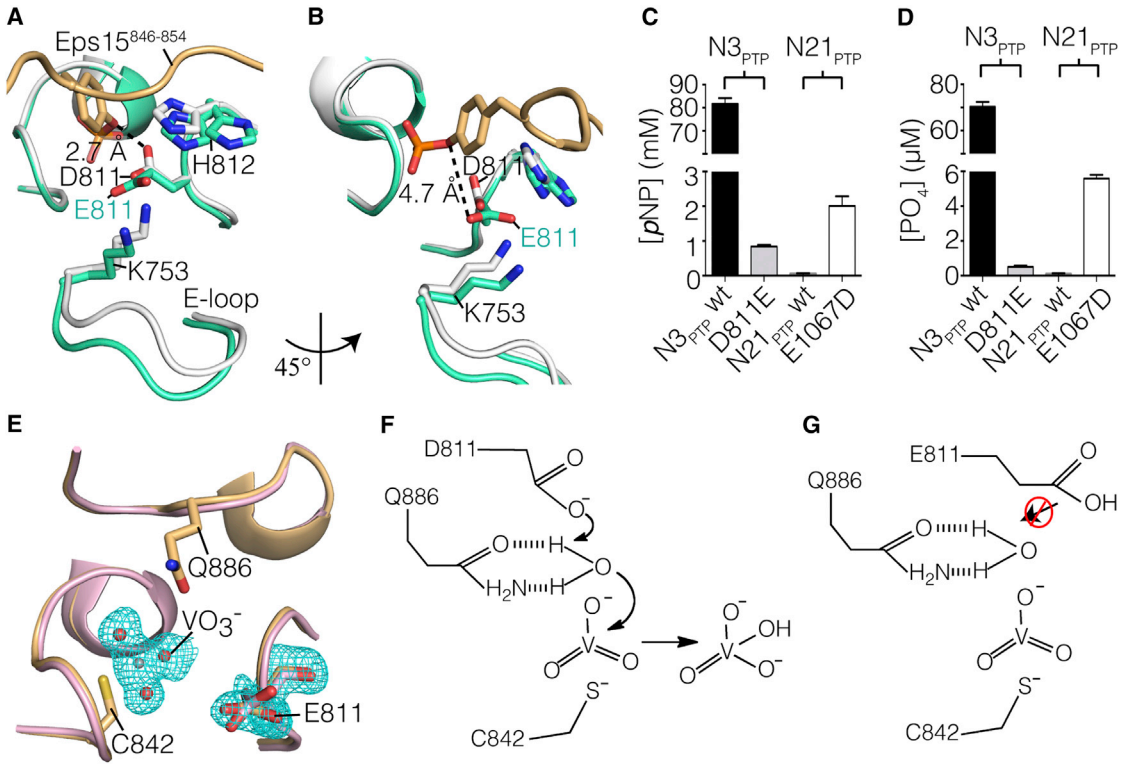

Figure 5. Effect of the D811E Substitution on the Substrate Recognition

(A) Close view of the $N3_{PTP}$ D811E/C842S-$Eps15^{846–854}$ complex structure (green cyan) active site pocket superposed with the $N3_{PTP}$ C842S mutant structure (PDB accession code 4QUN).

(B) Superposition rotated 45° around the horizontal axis of (A). Protonation distance of the tyrosyl leaving group of the substrate by the D811/E811 is 2.7 Å and 4.7 Å, respectively (blue dashed line).

(C) Phosphatase assay of wild-type ($N3_{PTP}$ wt) and D811E mutant of $N3_{PTP}$, wild-type ($N21_{PTP}$ wt) and E1067D mutant of $PTPN21_{PTP}$ using *p*NPP.

(D) $Eps15^{846–854}$ as the substrate. For the *p*NPP assay, 800 nM protein was mixed with 2 mM *p*NPP substrate. For the phosphopeptide assay, 200 nM protein and 200 μM $Eps15^{846–854}$ were used. Error bars represent the SEM for at least three independent assays.

(E) Close view of the $N3_{PTP}$ D811E mutant structure (light orange) active site pocket superposed with the $N3_{PTP}$ D811E/C842S-$Eps15^{846–854}$ complex structure. The trigonal planar shape of metavanadate is shown. The electron density corresponds to a simulated-annealing OMIT $F_o - F_c$ map contoured at 3σ.

(F) The proposal mechanism of orthovanadate formation in the active site of PTPN3.

(G) The formation of a metavanadate in the active site of PTPN3 D811E mutant.

See also Figure S6.

generate specific mutations (Stratagene). All primers used in the mutagenesis study are listed in Table S3. All of the mutations were confirmed using DNA sequencing.

Cell Culture, Transfection, Immunoprecipitation, and Immunoblotting

For immunoprecipitations, HEK293T or H1975 non-small-cell lung cancer cells that were transiently transfected with the indicated plasmids (wild-type, D811E, or H812F) were scraped from dishes into lysis buffer containing 50 mM Tris-HCl (pH 7.4), 150 mM NaCl, 1% NP40, 0.25% sodium deoxycholate, 1 mM EDTA, 10 mM NaF, 2 mM Na_3VO_4 1 mM PMSF, and protease inhibitor cocktail (Roche). For HEK293T cells, lysates were immunoprecipitated with an anti-Flag antibody and protein G-Sepharose beads (GE Healthcare) at 4°C for 3 hr. These beads were washed three times in lysis buffer before the addition of a DTT-containing sample buffer and boiling for 5 min. After resolution using SDS-PAGE, the immunoprecipitates were subjected to western blot analysis as previously described (Chen et al., 2012).

Protein Expression and Purification

His-tagged PTP constructs were expression in *Escherichia coli*, and purified by Ni-NTA resin (GE Healthcare) and size-exclusion chromatography. Additional details can be found in the Supplemental Experimental Procedures.

Crystallization and Data Collection

Protein crystallization trials were performed in 96-well plates using the sitting-drop vapor diffusion method at 20°C. In general, $N3_{PTP}$ D811A/C842S, $N3_{PTP}$ D811A/H812F/C842S/M883G, or $N3_{PTP}$ D811E/C842S was mixed with 10-fold molar excess of $Eps15^{846–854}$ solution to a final concentration of 8.5 mg/ml. Rod needle-shaped crystals were obtained from 1.5 μl of protein-peptide mixture and 0.5 μl of reservoir consisting of 100 mM Tris-HCl (pH 8.5), 21% PEG 8000, and 5% glycerol. $N3_{PTP}$ D811A/C842S in complex with $Eps15^{846–854}$ P850V was crystallized under the same conditions as described for $Eps15^{846–854}$, except that 26% PEG 8000 was used. To grow crystals of the $N3_{PTP}$ D811E mutant, a mixture containing a 9.5-fold molar excess of the Eps15 phosphopeptide plus a 0.5-fold molar excess of sodium orthovanadate was added to the $N3_{PTP}$ D811E mutant protein. The final concentration used for crystallization was 8.5 mg/ml. The best crystals of the $N3_{PTP}$ D811E mutant were grown under conditions similar to those used for the protein-peptide complex. Prior to data collection, all crystals excepted for $N3_{PTP}$ D811A/C842S in complex with $Eps15^{846–854}$ P850V were flash frozen in cryoprotectant solution consisting of 100 mM Tris-HCl (pH 8.5), 21% PEG 8000, and 8% glycerol.

Crystallization of the $N3_{PTP}$ Y676I mutant with a WPD loop in the close conformation was achieved by adding 5-fold molar excess of sodium orthovanadate to the purified $N3_{PTP}$ Y676I mutant to a final concentration of 8.0 mg/ml. The best crystals were grown in conditions consisting of 100 mM Tris-HCl (pH

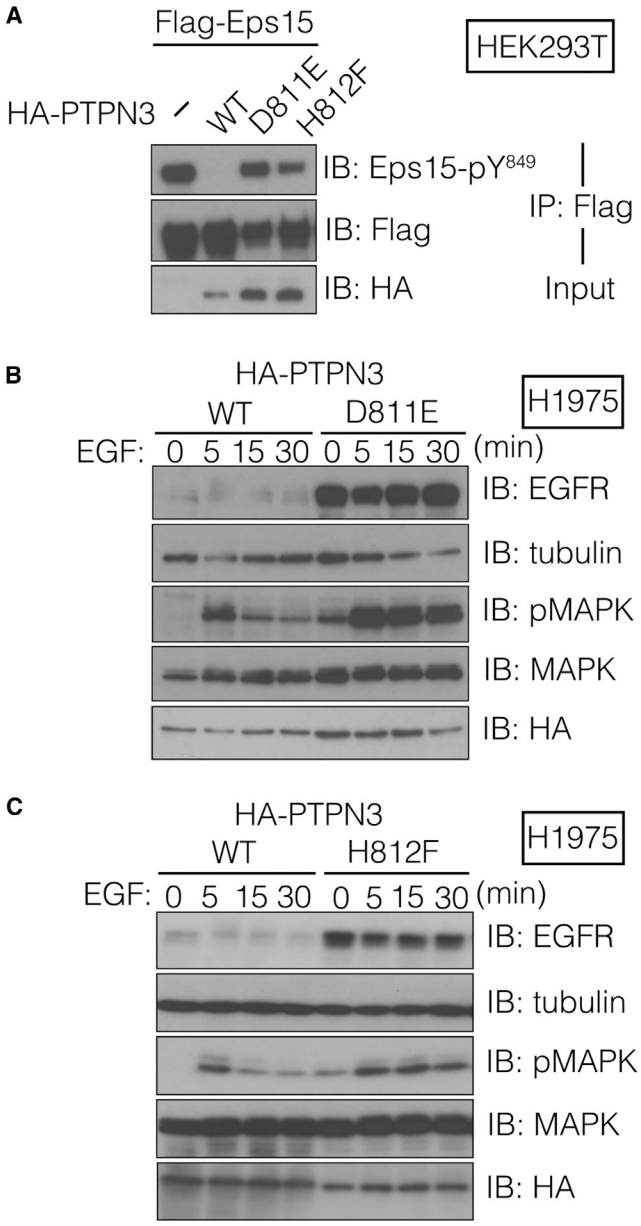

Figure 6. Effect of the Wild-Type and Mutants of PTPN3 on the Tyrosine Phosphorylation Levels of Eps15 upon EGF Stimulation

(A) Immunoprecipitation western analysis of wild-type, D811E, and H812F PTPN3 in HEK293T cells. Expression of wild-type PTPN3 markedly abolished EGF-induced tyrosine phosphorylation of Eps15 but not the D811E or the H812F mutants.

(B and C) Overexpression of D811E (B) or H812F (C) PTPN3 in H1975 lung cancer cells rescued endogenous EGFR protein levels and EGF-induced MAPK activation. The data shown are representative of three independent experiments.

7.5), 25% PEG 8000. Crystals of the $N3_{PTP}$ Y676I mutant were flash frozen in a cryoprotectant solution consisting of 100 mM Tris-HCl (pH 7.5), 26% PEG 8000, and 5% glycerol.

Structure Determination

X-Ray diffraction data of all six crystal structures were collected at the National Synchrotron Radiation Research Center BL-15A1 beamlines at a wavelength of 1.0 Å and recorded with a Rayonix MX300HE charge-coupled device area detector. Reflections were indexed, integrated, and scaled using HKL2000 (Otwinowski and Minor, 1997). The $N3_{PTP}$ D811A/C842S-$Eps15^{846–854}$ complex structure was determined by molecular replacement using Phaser (McCoy et al., 2007) and the wild-type $N3_{PTP}$ structure (PDB ID 2B49) as the search model. The best solutions for the other complexes were obtained using the $N3_{PTP}$ D811A/C842S-$Eps15^{846–854}$ complex structure as the search model (Table 1). The initial electron density map after Phenix refinement (Adams et al., 2010) guided the location of the PTP domain and $Eps15^{846–854}$. Waters were added using the ordered solvent process and the default parameters in Phenix were refined and manually checked from Coot (Emsley and Cowtan, 2004). The refined model was manually adjusted using Coot guided by $F_o - F_c$ difference maps. Coordinates for glycerol, sodium orthovandate, and sodium metavanadate were generated using LIBCHECK from Coot. The quality and geometry of the refined structures were evaluated using MolProbity (Chen et al., 2010). Data collection and refinement statistics are summarized in Table 1. Root-mean-square deviation (RMSD) was calculated using Dali (Holm and Rosenstrom, 2010) and molecular figures were generated using PyMOL.

Fluorescence Polarization

Fluorescence polarization assays were performed in a 30 μl volume containing 10 nM of N-terminal fluorescein isothiocyanate (FITC)-labeled Eps15 phosphopeptides and $N3_{PTP}$ D811A/C842S ranging from 8 μM to 0.488 nM in buffer containing 50 mM Tris-HCl (pH 7.4) and 150 mM NaCl. Reactions were repeated three times in 384-well black microplates and measured using a SpectraMax Paradigm plate reader (Molecular Devices) with excitation and emission wavelengths of 485 nm and 535 nm, respectively. Data were analyzed and plotted using Prism version 6.0d (GraphPad software).

*p*NPP Assay

*p*NPP assays were performed in a 50 μl volume comprising 50 mM Tris-HCl (pH 7.4), 50 mM NaCl, and 1–2 mM *p*NPP with varied concentrations of PTPs ranging from 50 nM to 800 nM. The reactions were incubated at 30°C for 10 min at 405 nm using a PowerWave XS2 microplate reader (BioTeK). The absorbance was converted to the amounts of *p*-nitrophenol produced using a standard curve of known amounts. Phosphatase activity was calculated from the three biological replicates.

Phosphopeptide Assay and Kinetic Analysis

For the phosphopeptide assay, 200 μl of reaction was set up containing 5–20 nM of purified proteins (excepted for the $PTPN3_{PTP}$ D811E mutant) in an assay buffer consisting of 50 mM Tris-HCl (pH 7.4), 50 mM NaCl, and 0–500 μM of indicated phosphopeptide. To measure the phosphatase activity of $N3_{PTP}$ D811E mutant, 2 μM purified protein was added. After 2–10 min incubation at 30°C, the reactions were terminated by adding 30 μl of phosphate reagent from the phosphate colorimetric assay kit (Biovision) following the manufacturer's instructions. The absorbance was measured at 650 nm, using a PowerWave XS2 microplate reader (BioTeK). Conversion of absorbance to the amounts of phosphate production was calculated using the standard curve of known phosphate concentrations. The data were fitted using a nonlinear curve and the kinetics parameters, K_m and k_{cat}, were calculated from the Michaelis-Menten equation using Prism version 6.0d (GraphPad software). All points in enzyme kinetics were measured in three replicates and the experiments were repeated three times to obtain consistent results.

ACCESSION NUMBERS

The atomic coordinates and structure factors for the $N3_{PTP}$ D811A/C842S-$Eps15^{846–854}$ complex, $N3_{PTP}$ D811A/C842S-$Eps15^{846–854}$ P850V complex, quadruple mutant-$Eps15^{846–854}$ complex, $N3_{PTP}$ D811E/C842S-$Eps15^{846–854}$ complex, $N3_{PTP}$ Y676I mutant, and $N3_{PTP}$ D811E mutant have been deposited in the RCSB PDB under accession codes 4RH5, 4S0G, 4RH9, 4RHG, 4RI4, and 4RI5, respectively.

SUPPLEMENTAL INFORMATION

Supplemental Information includes six figures, three tables, Supplemental Experimental Procedures, and three-dimensional molecular models and can be found with this article online at http://dx.doi.org/10.1016/j.str.2015.01.017.

ACKNOWLEDGMENTS

We would like to thank Yu-Ling Huang of the Institute of Biological Chemistry, Academia Sinica for the peptide synthesis. We thank the National Program for Biopharmaceuticals (NRPB, NSC 10102325-B-492-001) and the National Center for High-Performance Computing, National Applied Research Laboratories (NCHC, NAR Labs) of Taiwan for providing the computing resources. We thank Hui-Ling Shr of the National Core Facility for Protein Structural Analysis for crystallization screening. X-Ray data were collected on beamline BL-15A1 at the National Synchrotron Radiation Research Center, Taiwan.

Received: October 12, 2014
Revised: January 18, 2015
Accepted: January 24, 2015
Published: February 26, 2015

REFERENCES

Adams, P.D., Afonine, P.V., Bunkoczi, G., Chen, V.B., Davis, I.W., Echols, N., Headd, J.J., Hung, L.W., Kapral, G.J., Grosse-Kunstleve, R.W., et al. (2010). PHENIX: a comprehensive Python-based system for macromolecular structure solution. Acta Crystallogr. D Biol. Crystallogr. *66*, 213–221.

Andersen, J.N., Mortensen, O.H., Peters, G.H., Drake, P.G., Iversen, L.F., Olsen, O.H., Jansen, P.G., Andersen, H.S., Tonks, N.K., and Moller, N.P. (2001). Structural and evolutionary relationships among protein tyrosine phosphatase domains. Mol. Cell. Biol. *21*, 7117–7136.

Barr, A.J., Ugochukwu, E., Lee, W.H., King, O.N., Filippakopoulos, P., Alfano, I., Savitsky, P., Burgess-Brown, N.A., Muller, S., and Knapp, S. (2009). Large-scale structural analysis of the classical human protein tyrosine phosphatome. Cell *136*, 352–363.

Bentires-Alj, M., and Neel, B.G. (2007). Protein-tyrosine phosphatase 1B is required for HER2/Neu-induced breast cancer. Cancer Res. *67*, 2420–2424.

Berman-Golan, D., and Elson, A. (2007). Neu-mediated phosphorylation of protein tyrosine phosphatase epsilon is critical for activation of Src in mammary tumor cells. Oncogene *26*, 7028–7037.

Chen, V.B., Arendall, W.B., 3rd, Headd, J.J., Keedy, D.A., Immormino, R.M., Kapral, G.J., Murray, L.W., Richardson, J.S., and Richardson, D.C. (2010). MolProbity: all-atom structure validation for macromolecular crystallography. Acta Crystallogr. D Biol. Crystallogr. *66*, 12–21.

Chen, D.Y., Li, M.Y., Wu, S.Y., Lin, Y.L., Tsai, S.P., Lai, P.L., Lin, Y.T., Kuo, J.C., Meng, T.C., and Chen, G.C. (2012). The Bro1-domain-containing protein Myopic/HDPTP coordinates with Rab4 to regulate cell adhesion and migration. J. Cell Sci. *125*, 4841–4852.

Chen, K.E., Lin, S.Y., Wu, M.J., Ho, M.R., Santhanam, A., Chou, C.C., Meng, T.C., and Wang, A.H.J. (2014). Reciprocal allosteric regulation of p38 gamma and PTPN3 involves a PDZ domain-modulated complex formation. Sci. Signal. *7*, ra98.

Combet, C., Blanchet, C., Geourjon, C., and Deleage, G. (2000). NPS@: network protein sequence analysis. Trends Biochem. Sci. *25*, 147–150.

Confalonieri, S., Salcini, A.E., Puri, C., Tacchetti, C., and Di Fiore, P.P. (2000). Tyrosine phosphorylation of Eps15 is required for ligand-regulated, but not constitutive, endocytosis. J. Cell Biol. *150*, 905–912.

Critton, D.A., Tortajada, A., Stetson, G., Peti, W., and Page, R. (2008). Structural basis of substrate recognition by hematopoietic tyrosine phosphatase. Biochemistry *47*, 13336–13345.

Dadke, S., Cotteret, S., Yip, S.C., Jaffer, Z.M., Haj, F., Ivanov, A., Rauscher, F., 3rd, Shuai, K., Ng, T., Neel, B.G., et al. (2007). Regulation of protein tyrosine phosphatase 1B by sumoylation. Nat. Cell Biol. *9*, 80–85.

Elchebly, M., Payette, P., Michaliszyn, E., Cromlish, W., Collins, S., Loy, A.L., Normandin, D., Cheng, A., Himms-Hagen, J., Chan, C.C., et al. (1999). Increased insulin sensitivity and obesity resistance in mice lacking the protein tyrosine phosphatase-1B gene. Science *283*, 1544–1548.

Emsley, P., and Cowtan, K. (2004). Coot: model-building tools for molecular graphics. Acta Crystallogr. D Biol. Crystallogr. *60*, 2126–2132.

Francis, D.M., Rozycki, B., Koveal, D., Hummer, G., Page, R., and Peti, W. (2011). Structural basis of p38alpha regulation by hematopoietic tyrosine phosphatase. Nat. Chem. Biol. *7*, 916–924.

Francis, D.M., Kumar, G.S., Koveal, D., Tortajada, A., Page, R., and Peti, W. (2013). The differential regulation of p38alpha by the neuronal kinase interaction motif protein tyrosine phosphatases, a detailed molecular study. Structure *21*, 1612–1623.

Gingras, M.C., Zhang, Y.L., Kharitidi, D., Barr, A.J., Knapp, S., Tremblay, M.L., and Pause, A. (2009). HD-PTP is a catalytically inactive tyrosine phosphatase due to a conserved divergence in its phosphatase domain. PLoS One *4*, e5105.

Gray, C.H., Good, V.M., Tonks, N.K., and Barford, D. (2003). The structure of the cell cycle protein Cdc14 reveals a proline-directed protein phosphatase. EMBO J. *22*, 3524–3535.

Haj, F.G., Verveer, P.J., Squire, A., Neel, B.G., and Bastiaens, P.I. (2002). Imaging sites of receptor dephosphorylation by PTP1B on the surface of the endoplasmic reticulum. Science *295*, 1708–1711.

Han, S., Williams, S., and Mustelin, T. (2000). Cytoskeletal protein tyrosine phosphatase PTPH1 reduces T cell antigen receptor signaling. Eur. J. Immunol. *30*, 1318–1325.

Holm, L., and Rosenstrom, P. (2010). Dali server: conservation mapping in 3D. Nucleic Acids Res. *38*, W545–W549.

Hou, S.W., Zhi, H.Y., Pohl, N., Loesch, M., Qi, X.M., Li, R.S., Basir, Z., and Chen, G. (2010). PTPH1 dephosphorylates and cooperates with p38gamma MAPK to increase ras oncogenesis through PDZ-mediated interaction. Cancer Res. *70*, 2901–2910.

Julien, S.G., Dube, N., Read, M., Penney, J., Paquet, M., Han, Y., Kennedy, B.P., Muller, W.J., and Tremblay, M.L. (2007). Protein tyrosine phosphatase 1B deficiency or inhibition delays ErbB2-induced mammary tumorigenesis and protects from lung metastasis. Nat. Genet. *39*, 338–346.

Julien, S.G., Dube, N., Hardy, S., and Tremblay, M.L. (2011). Inside the human cancer tyrosine phosphatome. Nat. Rev. Cancer *11*, 35–49.

Klaman, L.D., Boss, O., Peroni, O.D., Kim, J.K., Martino, J.L., Zabolotny, J.M., Moghal, N., Lubkin, M., Kim, Y.B., Sharpe, A.H., et al. (2000). Increased energy expenditure, decreased adiposity, and tissue-specific insulin sensitivity in protein-tyrosine phosphatase 1B-deficient mice. Mol. Cell. Biol. *20*, 5479–5489.

Li, M.Y., Lai, P.L., Chou, Y.T., Chi, A.P., Mi, Y.Z., Khoo, K.H., Chang, G.D., Wu, C.W., Meng, T.C., and Chen, G.C. (2014). Protein tyrosine phosphatase PTPN3 inhibits lung cancer cell proliferation and migration by promoting EGFR endocytic degradation. Oncogene. . Published online September 29, 2014. http://dx.doi.org/10.1038/onc.2014.312.

Liu, X., Yang, N., Figel, S.A., Wilson, K.E., Morrison, C.D., Gelman, I.H., and Zhang, J. (2013). PTPN14 interacts with and negatively regulates the oncogenic function of YAP. Oncogene *32*, 1266–1273.

McCoy, A.J., Grosse-Kunstleve, R.W., Adams, P.D., Winn, M.D., Storoni, L.C., and Read, R.J. (2007). Phaser crystallographic software. J. Appl. Crystallogr. *40*, 658–674.

Mustelin, T., Vang, T., and Bottini, N. (2005). Protein tyrosine phosphatases and the immune response. Nat. Rev. Immunol. *5*, 43–57.

Ostman, A., Hellberg, C., and Bohmer, F.D. (2006). Protein-tyrosine phosphatases and cancer. Nat. Rev. Cancer *6*, 307–320.

Otwinowski, Z., and Minor, W. (1997). Processing of X-ray diffraction data collected in oscillation mode. Methods Enzymol. Macromol. Crystallogr. A *276*, 307–326.

Pannifer, A.D., Flint, A.J., Tonks, N.K., and Barford, D. (1998). Visualization of the cysteinyl-phosphate intermediate of a protein-tyrosine phosphatase by x-ray crystallography. J. Biol. Chem. *273*, 10454–10462.

Phan, J., Lee, K., Cherry, S., Tropea, J.E., Burke, T.R., and Waugh, D.S. (2003). High-resolution structure of the *Yersinia pestis* protein tyrosine phosphatase YopH in complex with a phosphotyrosyl mimetic-containing hexapeptide. Biochemistry *42*, 13113–13121.

Ren, L., Chen, X., Luechapanichkul, R., Selner, N.G., Meyer, T.M., Wavreille, A.S., Chan, R., Iorio, C., Zhou, X., Neel, B.G., et al. (2011). Substrate specificity of protein tyrosine phosphatases 1B, RPTPalpha, SHP-1, and SHP-2. Biochemistry *50*, 2339–2356.

Salmeen, A., Andersen, J.N., Myers, M.P., Tonks, N.K., and Barford, D. (2000). Molecular basis for the dephosphorylation of the activation segment of the insulin receptor by protein tyrosine phosphatase 1B. Mol. Cell *6*, 1401–1412.

Sarmiento, M., Zhao, Y., Gordon, S.J., and Zhang, Z.Y. (1998). Molecular basis for substrate specificity of protein-tyrosine phosphatase 1B. J. Biol. Chem. *273*, 26368–26374.

Stols, L., Gu, M., Dieckman, L., Raffen, R., Collart, F.R., and Donnelly, M.I. (2002). A new vector for high-throughput, ligation-independent cloning encoding a tobacco etch virus protease cleavage site. Protein Expr. Purif. *25*, 8–15.

Streuli, M., Krueger, N.X., Thai, T., Tang, M., and Saito, H. (1990). Distinct functional roles of the two intracellular phosphatase like domains of the receptor-linked protein tyrosine phosphatases LCA and LAR. EMBO J. *9*, 2399–2407.

Tiganis, T., and Bennett, A.M. (2007). Protein tyrosine phosphatase function: the substrate perspective. Biochem. J. *402*, 1–15.

Tonks, N.K. (2006). Protein tyrosine phosphatases: from genes, to function, to disease. Nat. Rev. Mol. Cell Biol. *7*, 833–846.

van Bergen En Henegouwen, P.M. (2009). Eps15: a multifunctional adaptor protein regulating intracellular trafficking. Cell Commun. Signal. *7*, 24.

Villa, F., Deak, M., Bloomberg, G.B., Alessi, D.R., and van Aalten, D.M. (2005). Crystal structure of the PTPL1/FAP-1 human tyrosine phosphatase mutated in colorectal cancer: evidence for a second phosphotyrosine substrate recognition pocket. J. Biol. Chem. *280*, 8180–8187.

Wadham, C., Gamble, J.R., Vadas, M.A., and Khew-Goodall, Y. (2003). The protein tyrosine phosphatase Pez is a major phosphatase of adherens junctions and dephosphorylates beta-catenin. Mol. Biol. Cell *14*, 2520–2529.

Wang, Y., and Pallen, C.J. (1991). The receptor-like protein tyrosine phosphatase HPTP alpha has two active catalytic domains with distinct substrate specificities. EMBO J. *10*, 3231–3237.

Yu, X., Chen, M., Zhang, S., Yu, Z.H., Sun, J.P., Wang, L., Liu, S., Imasaki, T., Takagi, Y., and Zhang, Z.Y. (2011). Substrate specificity of lymphoid-specific tyrosine phosphatase (Lyp) and identification of Src kinase-associated protein of 55 kDa homolog (SKAP-HOM) as a Lyp substrate. J. Biol. Chem. *286*, 30526–30534.

Zhang, S.H., Liu, J., Kobayashi, R., and Tonks, N.K. (1999). Identification of the cell cycle regulator VCP (p97/CDC48) as a substrate of the band 4.1-related protein-tyrosine phosphatase PTPH1. J. Biol. Chem. *274*, 17806–17812.

Zhang, P., Guo, A., Possemato, A., Wang, C., Beard, L., Carlin, C., Markowitz, S.D., Polakiewicz, R.D., and Wang, Z. (2013). Identification and functional characterization of p130Cas as a substrate of protein tyrosine phosphatase nonreceptor 14. Oncogene *32*, 2087–2095.

Zheng, X.M., Resnick, R.J., and Shalloway, D. (2000). A phosphotyrosine displacement mechanism for activation of Src by PTPalpha. EMBO J. *19*, 964–978.

